Research Article

Journal of Environmental Nanotechnology

Predictive Optimization of Electroless Coating Parameters for AH36 Steel in Defence Marine Applications

Ganta Suresh[1], T. Vinod Kumar[1*], R. Muraliraja[1*] and S. Padmanabhan[2]

[1]Department of Mechanical Engineering, Vels Institute of Science, Technology and Advanced Science (VISTAS), Chennai, TN, India
[2]Department of Mechanical Engineering, Vel Tech Rangarajan Dr. Sagunthala R&D Institute of Science and Technology, Chennai, TN, India
Received: 12.11.2025 Accepted: 26.11.2025 Published: 30.12.2025
*vinod.se@vistas.ac.in and muralimechraja@gmail.com

ABSTRACT

The present study concerns the parametric predictive optimization of electroless nickel-phosphorus coating on AH36 steel, which is commonly utilized in defence marine sector. Three process factors, namely, nanoparticle quantity, surfactant concentration, and reducing agent, were considered at four levels to identify their effect on coating thickness and surface roughness. Experiment was based on orthogonal array L16 and analysed by Taguchi method and Grey Relational Grade (GRG) to elicit the optimal conditions. Signal-to-noise (S/N) ratio analysis indicated that the nanoparticles were the most significant process parameter for film thickness, and the reducing agent for surface roughness. Regression models predicting coating properties were established and the significance level of parameters was confirmed by ANOVA. A confirmation test was conducted, and the substrate was evaluated using Scanning Electron Microscopy (SEM), Energy Dispersive X-ray Analysis (EDX), X-ray Diffraction (XRD), coating thickness measurement, and surface roughness analysis. The results showed that the optimized process parameters, A4B3C3 (1.5g of TiO_2, 1.2 g of surfactant and 40 g of reducing agent) led to a significant enhancement in coating performance, confirming the potential of the technique for improving the surface properties of AH36 steel for marine defence applications. A maximum coating thickness of 30 microns per hour was achieved, which is reported for the first time. A pore-free, smooth surface was observed through SEM analysis. The distribution of the added nanoparticles was homogeneous, as reported in the EDX analysis. The presence of TiO_2 was further confirmed by the XRD diffraction peaks.

Keywords: Electroless coating; AH36 steel; Taguchi method; Grey relational grade; Surface roughness optimization.

1. INTRODUCTION

High-performance materials are essential to withstand severe corrosion and mechanical wear encountered in naval engineering and marine defence applications. AH36 steel, a high-strength structural steel certified by shipbuilding classification societies, is widely used in the fabrication of ship hulls and structures due to its excellent mechanical properties, such as high yield strength and toughness (Selvan *et al.* 2023). Despite these advantages, AH36 steel suffers from poor corrosion resistance in aggressive marine environments, threatening structural safety and reducing service life (Selvan *et al.* 2022). To mitigate this drawback, protective surface coatings have become critical in extending the durability and functionality of marine-grade steels. Among various techniques, electroless nickel-phosphorus (Ni-P) plating has attracted significant interest due to its uniform coating thickness, ability to cover complex geometries, and high corrosion and wear resistance. Unlike electroplating, electroless deposition does not require an external power source; it relies on a controlled chemical reduction reaction to deposit a metallic layer, making it highly suitable for defence marine components (Hao *et al.* 2024).

The quality and performance of Ni-P coatings are significantly influenced by process parameters including the concentrations of nanoparticles, surfactants, and reducing agents. Nanoparticles such as TiO_2, SiC, and Al_2O_3 enhance hardness, wear resistance, and corrosion resistance. Surfactants are critical in dispersing and stabilizing these nanoparticles, preventing agglomeration, and promoting uniform distribution throughout the coating (Krishnakumar and Elansezhian, 2020). Reducing agents like sodium hypophosphite control both the deposition rate and the phosphorus content of the coating, thereby affecting ductility and corrosion behaviour. To optimize these variables, the present study employed a Taguchi Design of Experiments approach using an Orthogonal Array that minimizes the number of experimental runs while capturing the interactions between parameters. When combined with Grey Relational Analysis (GRA), this method supports multi-objective optimization for simultaneously maximizing coating thickness and minimizing surface

roughness. These responses are vital indicators of coating performance, influencing marine biofouling, drag resistance, and fatigue behaviour (Rosas-Laverde *et al.* 2020). The inclusion of TiO_2 nanoparticles in Ni-P coatings has shown considerable promise in enhancing mechanical and corrosion properties (Kuo *et al.* 2008). Studies report that Ni-P- TiO_2 coatings exhibit improved wear and stress corrosion cracking resistance, especially in saline environments such as 3.5% NaCl solutions (Zhang *et al.* 2019; Hadipour *et al.* 2015; Senthilkumar *et al.* 2021; Venkatesh and Venkatesan, 2015). The formation of a TiO_2 layer leads to more uniform surface coverage, fewer cracks, and higher hardness. Optimal Ti concentrations (e.g., 0.5 g/L) resulted in a microhardness of 675 Hv and corrosion inhibition efficiency of 96.4% (Shahzad *et al.* 2020). Heat treatment further transforms amorphous structures into crystalline Ni_3P and Ni_3Ti phases, boosting hardness and corrosion resistance (Zhang *et al.* 2019). Additional advancements include duplex Ni-P-TiO_2/Ni-P coatings that combine high-phosphorus inner layers with titania-reinforced outer layers for superior protection. Applications on substrates like AZ91D magnesium alloys have demonstrated enhanced performance, including 613 VHN hardness and a corrosion rate reduction of 82% at 12.5 g/L TiO_2.

This study aims to develop predictive models using regression and ANOVA to correlate process inputs with coating responses. Surface characterization was conducted using SEM, EDAX, XRD, and measurements of coating thickness and roughness.

2. EXPERIMENTAL DETAILS AND PROCEDURE

AH36 steel is a normal high strength structural steel used in ship construction and marine engineering. It generally uses loss of ferromagnetic properties as an index of low carbon equivalent. The typical chemical compositions of AH36 include carbon (0.18%), manganese (0.90–1.60%) and silicon (0.50%). It also includes phosphorous (0.035%) and sulphur (0.035%). Nickel is added to the backing material (up to 0.40%) to improve hot workability and in turn, enhance corrosion resistance and other mechanical properties required for submarine defence applications. The substrates were formed into cylinders measuring 20 mm in diameter and 7 mm in thickness. The specimens were first metallographically ground using a surface grinding machine and then finely polished with a disc polisher. Substrates were pre-treated before coating to eliminate impurities and surface activation. The process included degreasing in acetone for 3 minutes, cleaning with ethanol for additional 3 minutes, and dipping in a 20% sulphuric acid solution for 30 seconds. After each step, the samples were washed with deionized water. Finally, the substrates were dipped in the electroless plating solution.

Bath solution comprised of nickel sulphate 30 g/L (as Ni source), sodium hypophosphite 40 g/L (as reducing agent), sodium citrate 25 g/L (as complexing agent) and ammonium acetate 50 g/L (as buffer). Sodium dodecyl sulphate (particle size <50 nm), purchased from Sigma-Aldrich, was added as a surfactant. The pH was adjusted to 8 using liquid ammonia. Coating was carried out in a 250 mL glass beaker at 85 ℃ for 1 h. The surfactant was predissolved in 1 L of distilled water under magnetic stirring at various concentrations. At the beginning of the deposition, the surfactant solution was added dropwise to the bath solution five times using a pipette. Co-deposition of nano-TiO_2 particles was performed under continuous magnetic stirring in order to keep the nanoparticles suspended and to ensure a homogeneous distribution during deposition. The coated substrates were dried and stored in a desiccator to minimize oxidation on the coated film for analysis.

To measure the coating thickness of an electroless-coated substrate using the weight gain method, first weigh the substrate before coating to obtain the initial weight W1, then weigh it after coating to get the final weight W2. The weight gain is calculated as $\Delta W = W2 - W1$. Using the known density ρ of the coating material (in g/cm³) and the surface area A of the substrate (in cm²), the coating thickness t can be determined using the equation in cm

$$t = \frac{\Delta W}{\rho . A} \quad \ldots(1)$$

Surface roughness was measured using a handheld portable surface tester (Model: SJ-210, retractable type) and the acquired surface profile data was captured and analysed using Surftest SJ USB Communication Tool software (Version 5.006). The surface morphology of the deposit was confirmed with a scanning electron microscope (SEM) (Hitachi, Model: S-3400 N operating at an accelerating voltage of 15 kV) to ascertain uniform and pore free deposit. Energy Dispersive X-ray Analysis was used as a supplementary technique to identify the elemental composition of the deposits and to verify the dispersion of the nano particles added. The crystalline structure of the deposited coatings was analyzed using X-ray Diffraction (XRD) with a Rigaku Ultima IV diffractometer equipped with a copper (Cu) anode. The scan was performed in steps of 0.02° per second over a 2θ range of 10° to 90°. The interfacial adhesion between the coating and the substrate was evaluated following the VDI 3198 standard, using a Rockwell hardness tester equipped with a C-type diamond cone indenter and applying a load of 150 kg.

In the present work, the effects of three significant process variables at four levels on the electroless deposition were studied. The concentration of the nanoparticles was varied at 0 g, 0.5 g, 1 g and 1.5 g, while that of the surfactant was fixed at 0 g, 1 g, 1.2 g, 1.6 g, and at the same time the concentration of the

reducing agent (e.g., sodium hypophosphite) was 30 g, 35 g, 40 g, and 45 g for each experiment The purpose of these changes was to examine the independent and combined effects of these variations on the characteristic and quality of the electroless coatings reported in Table 1.

Table 1. Selection of variables and their levels

Variables	Units	Level 1	Level 2	Level 3	Level 4
Nanoparticles (A)	g	0	0.5	1	1.5
Surfactant (B)	g	0	0.6	1.2	1.8
Reducing agent (C)	g	30	35	40	45

3. RESULTS AND DISCUSSION

The orthogonal array-based design of experiment was employed to systematically study the effects of three process variables nanoparticles, surfactant, and reducing agent on two key responses coating thickness and surface roughness. Each variable was tested at four levels, and a total of 16 experimental runs were conducted shown in the Table 2.

Table 2. Orthogonal array-based experimental design

S. No.	Nano-particles (g)	Surfactant (g)	Reducing Agent (g)	Coating Thickness (µ)	Surface Roughness (R_a)
1	0	0	30	18	1.85
2	0	1	35	22	2.1
3	0	1.2	40	25	1.65
4	0	1.6	45	23	2.35
5	0.5	0	35	20	1.2
6	0.5	1	30	19	1.95
7	0.5	1.2	45	19	2
8	0.5	1.6	40	20	1.55
9	1	0	40	20	2.25
10	1	1	45	21	1.45
11	1	1.2	30	22	1.3
12	1	1.6	35	22	1.9
13	1.5	0	45	21	1.75
14	1.5	1	40	28	2.4
15	1.5	1.2	35	27	1.5
16	1.5	1.6	30	23	1.25

Minitab software was used to analyze the signal-to-noise (S/N) ratios for the coating thickness data based on the "larger is better" criterion and surface roughness on the “smaller is better”. The calculated delta values, representing the range of influence of each factor as shown in Table 3, were highest for nanoparticles (1.58), followed by surfactant (1.72), and then reducing agent (1.86). Based on these results, nanoparticles were ranked as the most influential factor affecting coating thickness, with surfactant second and reducing agent third (Jeyaganesh *et al.* 2021).

Table 3. Response table for signal to noise ratios

Level	Nanoparticles	Surfactant	Reducing Agent
1	-5.890	-4.708	-3.840
2	-4.303	-5.769	-4.281
3	-4.531	-4.043	-5.701
4	-4.481	-4.685	-5.383
Delta	1.587	1.726	1.861
Rank	3	2	1

The delta values, indicating the range of influence for each factor, were highest for the reducing agent (1.861), followed by surfactant (1.726), and then nanoparticles (1.587). Accordingly, the reducing agent was ranked as the most significant factor affecting surface roughness, with surfactant second and nanoparticles third.

This article reports the combined effect of nanoparticles, surfactant and reducing agent on coating thickness and surface roughness by the use of GRA, as shown in Table 4. The S/N ratios were normalized for both response and converted into Grey relational coefficients (Δklm). For each experimental run, the weighted Grey relational grade was computed. Extreme coating thickness and the minimal surface roughness indicate the best performance. The best Grey relational grade (0.76) was achieved under the conditions of 1.5 g nanoparticles, 1 g surfactant and 40 g reducing agent out of the 16 trails. Further performing conditions were 1.5 g of nanoparticles; 1.2 g of surfactant and 35 g of reducing agents (0.58, rank 4) and 1 g nanoparticles; 1.6 g of surfactant and 35 g of reducing agents (0.66, rank 3). Trials of a lower rank tended to have a lower coat thickness and/or a higher surface roughness, indicating that all three parameters had to be optimized simultaneously.

Table 4. Grey relational grade and its ranking

Variables and Responses						S/N ratio		Normalization		Converting Normalized Value Into Δklm		Grey Relational Grade	
S. No	Nano-particles	Surfactant	Reducing Agent	Coating Thickness	Surface Roughness	Coating Thickness	Surface Roughness	Coating Thickness	Surface Roughness	Coating Thickness	Surface Roughness	Weightage	Rank
1	0	0	30	18	1.85	25.11	-5.34	0.00	0.46	0.33	0.48	0.41	12
2	0	1	35	22	2.1	26.85	-6.44	0.40	0.46	0.45	0.48	0.47	10
3	0	1.2	40	25	1.65	27.96	-4.35	0.70	0.25	0.63	0.40	0.51	8
4	0	1.6	45	23	2.35	27.23	-7.42	0.50	0.63	0.50	0.57	0.54	7
5	0.5	0	35	20	1.2	26.02	-1.58	0.20	0.04	0.38	0.34	0.36	16
6	0.5	1	30	19	1.95	25.58	-5.80	0.10	1.00	0.36	1.00	0.68	2
7	0.5	1.2	45	19	2	25.58	-6.02	0.10	0.38	0.36	0.44	0.40	14
8	0.5	1.6	40	20	1.55	26.02	-3.81	0.20	0.33	0.38	0.43	0.41	13
9	1	0	40	20	2.25	26.02	-7.04	0.20	0.71	0.38	0.63	0.51	9
10	1	1	45	21	1.45	26.44	-3.23	0.30	0.13	0.42	0.36	0.39	15
11	1	1.2	30	22	1.3	26.85	-2.28	0.40	0.79	0.45	0.71	0.58	6
12	1	1.6	35	22	1.9	26.85	-5.58	0.40	0.92	0.45	0.86	0.66	3
13	1.5	0	45	21	1.75	26.44	-4.86	0.30	0.42	0.42	0.46	0.44	11
14	1.5	1	40	28	2.4	28.94	-7.60	1.00	0.54	1.00	0.52	0.76	1
15	1.5	1.2	35	27	1.5	28.63	-3.52	0.90	0.00	0.83	0.33	0.58	4
16	1.5	1.6	30	23	1.25	27.23	-1.94	0.50	0.75	0.50	0.67	0.58	5

This means that the nanoparticle and surfactant are significantly positive and strong factors affecting the thickness of coating and reducing agent has little effect (Table 5). The output from ANOVA indicates that the F-value is 1.89; while the p-value is 0.185, which means the regression model is not statistically significant at 95% confidence level. Nanoparticles ($F = 2.95$, $p = 0.111$) and surfactant ($F = 2.60$, $p = 0.133$) both have only a weak but insignificant influence on coating thickness, while the reducing agent addition ($F = 0.12$, $p = 0.737$) shows no significant effect. The variation is mainly covered by the error term, suggesting other factors may be responsible for coating thickness (Zhu *et al.* 2025). The regression equation developed to predict coating thickness is

Coating thickness=17.18 + 2.00 Nanoparticles + 1.78 Surfactant + 0.040 Reducing agent

Table 5. Analysis of Variance for coating thickness

Source	DF	Adj SS	Adj MS	F-value	P-value
Regression	3	38.428	12.8092	1.89	0.185
Nanoparticles	1	20.000	20.0000	2.95	0.111
Surfactant	1	17.628	17.6277	2.60	0.133
Reducing agent	1	0.800	0.8000	0.12	0.737
Error	12	81.322	6.7769		
Total	15	119.750			

The regression equation for surface roughness is given by

Surface Roughness=1.016 - 0.148 Nanoparticles - 0.019 Surfactant + 0.0238 Reducing agent

Table 6. Analysis of Variance for surface roughness

Source	DF	Adj SS	Adj MS	F-Value	P-Value
Regression	3	0.39289	0.130964	0.85	0.491
Nano-particles	1	0.10878	0.108781	0.71	0.416
Surfactant	1	0.00208	0.002078	0.01	0.909
Reducing agent	1	0.28203	0.282031	1.84	0.200
Error	12	1.84195	0.153496		
Total	15	2.23484			

This equation suggests that increasing nanoparticle and surfactant concentrations tends to reduce surface roughness, while the reducing agent slightly increases it as shown in the Table 6. The ANOVA results indicate that the overall model is not statistically significant (F-value = 0.85, p = 0.491). Individually, none of the factors have a significant effect on surface roughness at 95% confidence level, with nanoparticles (p = 0.416), surfactant (p = 0.909), and reducing agent (p =

0.200) all showing p-values above 0.05. The error term accounts for most of the variability, implying that additional factors may influence surface roughness beyond those studied (Vijayanand *et al.* 2021).

The main effect plot for S/N ratios in Fig. 1 shows the effect of some process parameters of nanoparticles, surfactant, and reducing agent on the coating quality where lower-the-better criterion for response is considered. The average S/N ratios for the different levels are represented in the plot. For nanoparticles, a concentration increase of 0–0.5 wt.% is realized. The pattern of the S/N ratio increases as the wt. % increases (with deteriorating effect beyond 0.5 wt. %) signifying good coating performance. For the cationic surfactant, the S/N ratio diminishes at 0.1 wt. % and peaks at 1.0 wt. % which correlates to a minimum concentration to decrease surface roughness or defect. The dependence of the S/N ratio with the reducing agent concentration exhibits a peak maximum at 30 g/L and decreases with surfactant concentration, showing a minimum at 40 g/L, suggesting that high reducing agent concentrations might cause instability of the bath or deposition. The optimum levels for improved coating performance, as deduced from the higher S/N ratios, are apparently 0.5 wt. % nanoparticles, 1.0 wt. % surfactant, and 30 g/L reductant (Salicio-Paz *et al.* 2021).

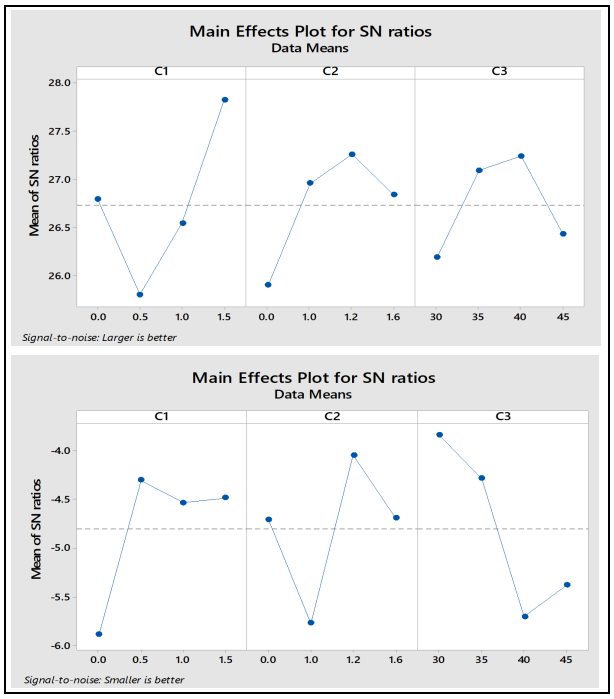

Fig. 1: Main effects plot for the signal-to-noise

The residual plots for the S/N ratios assess the adequacy and assumptions of the underlying statistical model shown in Fig. 2. The normal probability plot shows that the residuals closely follow a straight line, indicating that they are approximately normally distributed. The residuals *versus* fits plot displays a random scatter without any discernible pattern, suggesting homoscedasticity and confirming that the residuals have constant variance across all fitted values. The histogram of residuals is roughly symmetric and centered around zero, further supporting the assumption of normality. Lastly, the residuals *versus* observation order plot shows no systematic trend or pattern, implying the absence of autocorrelation in the experimental data (Sarkar *et al.* 2020).

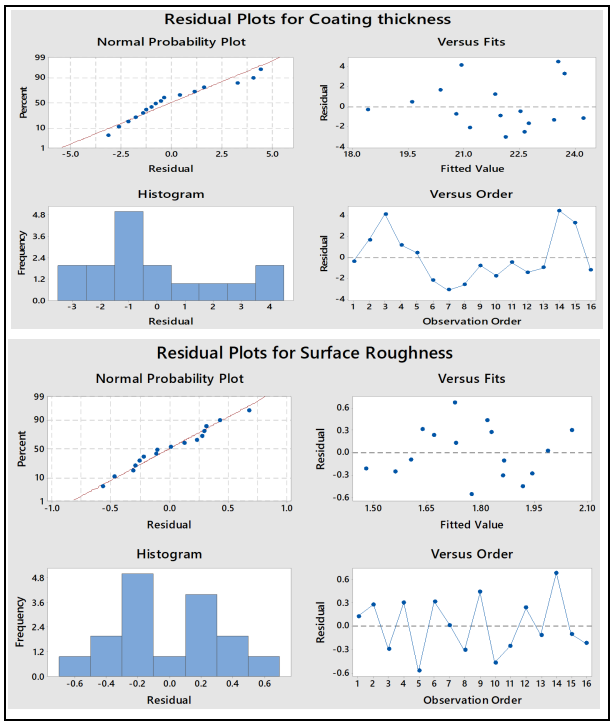

Fig. 2: Residual plots for coating thickness and surface roughness

Fig. 3 shows the contour mesh plots of combined effect of the process parameters (reducing agent, surfactant, and nanoparticles) on the coating thickness and surface roughness of the electroless coatings. Fig. 3 clearly shows that a lower concentration (<35 g/L) provides a better balance between coating thickness and surface roughness, as indicated by the dense blue region corresponding to low roughness. When the concentration of reducing agent exceeds 40 g/L, the coating surface becomes significantly rougher and the coating thickness becomes more irregular. This indicates that over-reduction and non-uniform deposition are major factors contributing to this effect. In the surfactant graph, the ideal coating properties are found within the surfactant concentration of 0.5–1.0 wt. %, where the surface roughness is the lowest and the thickness of the coating is within a reasonable value. Lower surfactant concentration (<0.5 wt. %) results in sparse and irregular coating. Higher concentrations (1.25 wt. %) did not contribute to any improvement, instead, they deteriorated the surface condition due to micelle formation or bath instability.

The contour plot of the nanoparticles discloses that low additions (approximately 0.5–1.0 wt. %) transferred onto the substrate conversely lead to better coating uniformity and acceptable surface roughness. At low and high ranges of nanoparticle level, the surface roughness gets quite higher and coating thickness more irregular because of poor dispersion or particle agglomeration.

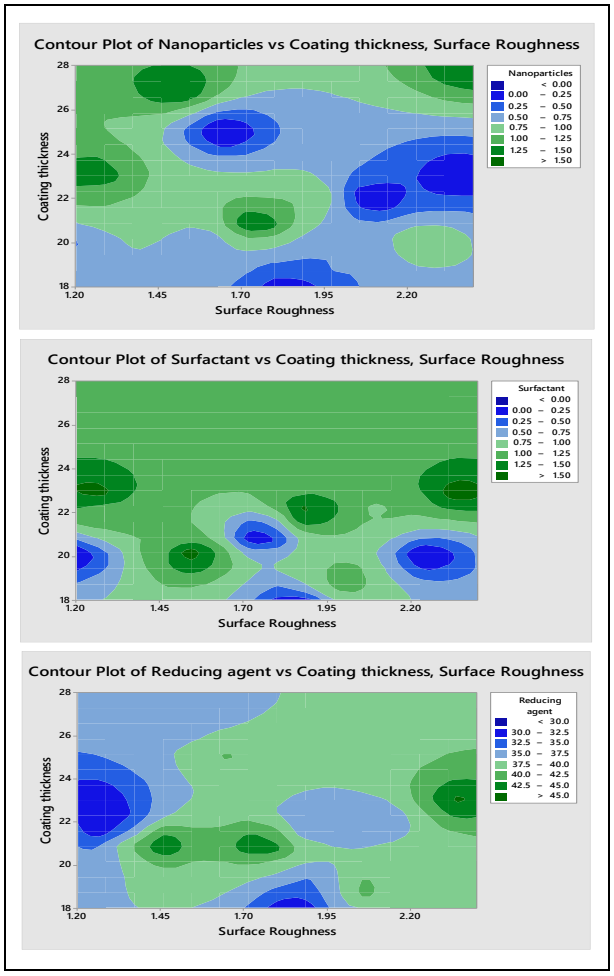

Fig. 3: Contour plots for various process parameters

Fig. 4 shows the 3D graph of Coating Thickness, Surface roughness using three different parameters (reducing agent, surfactant, nanoparticle). The surface plot of Reducing Agent *versus* Coating Thickness and Surface Roughness is a smooth yet fluctuating surface implying that both the thickness and roughness of the coating affect the quantity of the reducing agent. The spread is more marked in the surface roughness direction, indicating a more important effect of this parameter. The second plot shows similar results for Surfactant, that also presents complex surface structures and a little less variation than reducing agent, similar to the results obtained by Srivastwa *et al.* (2022). This moderate dependence of surfactant concentration on coating thickness and surface roughness means that surfactant concentration can be controlled over the same ranges. In the case of Nanoparticles, the surface plot shows sharp regions and oscillating patterns, which indicate a strong sensitivity to both parameters. The large peaks and valleys on the surface imply that nanoparticle distribution is heavily influenced by the interplay between surface roughness and coating thickness.

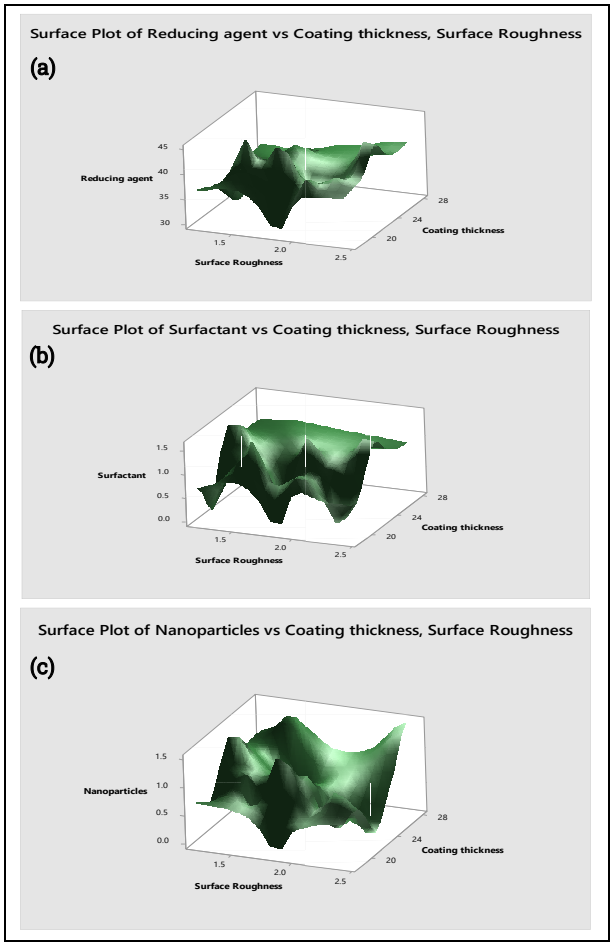

Fig. 4: Relationship between coating thickness and surface roughness on variables

The interaction plots of Coating Thickness and Surface Roughness give the complete understanding of the synergistic effects of Nanoparticles, Surfactant and Reducing Agen. Fig. 5 shows the relationship between coating thickness and the three variables is complex. Large nanoparticle amounts reflect an increase in the coating thickness, especially when associated with high values for the surfactant or reducer, which is shown by the asymmetrical curves. The existence of distinct non-parallel lines in several of the plots indicates a strong interaction effect suggesting that the effect of one factor is related to the level of the other factors. The plot of interaction for Surface Roughness also exhibits such kind of complexity (Fig. 6). The response is seen to be very sensitive to all the three variables and with a more erratic trends across the panels especially in the combinations involving droplet and surfactant level. Nonlinearity and

cross terms are observed frequently, showing strong interaction effects and suggesting that surface roughness is not entirely determined based on one factor alone. Instead, the product is closely related to the ratio of NP–surfactant concentration to the concentration of the reducing agent.

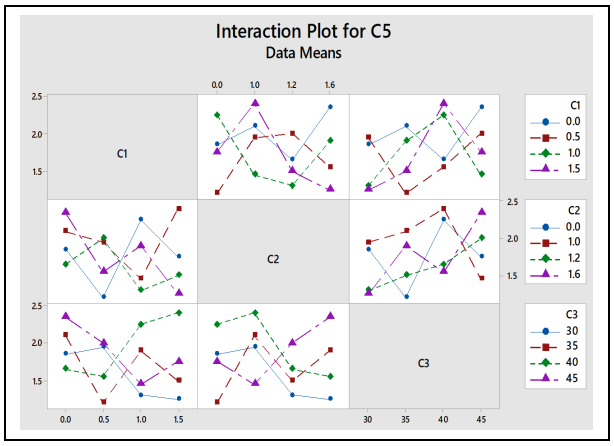

Fig. 5: Interaction plot for surface roughness

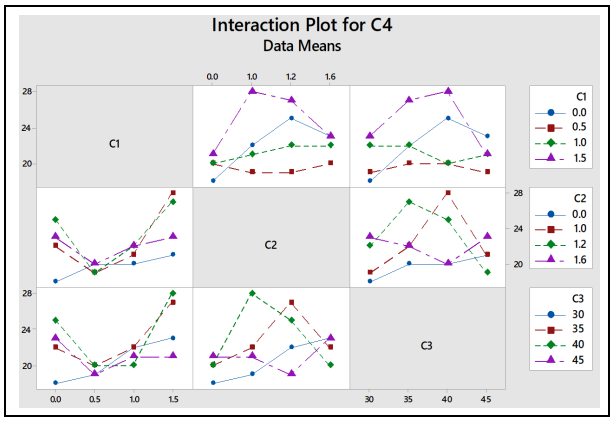

Fig. 6: Interaction plot for coating thickness

4. CONFIRMATION EXPERIMENT AND VALIDATION

According to the optimum levels obtained from GRA and regression, the validation experiment was achieved using GA4RB3C2 (1.5 g of NP, 1.2 g of surfactant, and 40 g of reducing agent). This sample showed improvement in the thickness and the surface roughness of the coating, compared to the other samples. The thickness layer was higher (30 µm) than the average response measured for the initial experimental design, while the R_a was much lower, which suggested the adhesion of a smoother and more regular deposit. Scanning electron microscopy showed that TiO_2 nanoparticles were uniformly distributed on the coated layer resulting in more homogenous microstructure, providing better mechanical properties. The EDS mapping further indicated the homogeneous distributions of Ni, P, Ti elements in the matrix, which demonstrated that the introduction of nanoparticles was successful into Ni-P coating layer.

The SEM image of a Ni-P-TiO_2 electroless coated surface is shown in Fig. 7 (250×magnification with a 200 µm scale bar). The nodular surface morphology characteristic of electroless Ni-P deposits is observed in the coating. These nodules form a spherical to hemispherical shape, suggesting high uniform growth and stable deposition conditions. Such morphology benefits both uniform distribution of Ni-P nodules or dispersed TiO_2 particles (Thiemig and Bund, 2008). Size distribution of the particles, computed from the image, indicates that the size varies from 5 µm to 50 µm and most percentage of the particles are between 10 and 30 µm. This suggests a bimodal distribution, perhaps as a result of the co-deposition of agglomerated TiO_2 nanoparticles or clusters in the Ni-P matrix. It is suggested that the bigger ones are nucleation sites or preferential growth zones and the smaller ones are inclusions of TiO_2 or finer Ni-P grains. Particulate TiO_2 seems uniformly distributed on the surface, as no large aggregates or clumping formation are observable even at a comparatively low magnification. This indicates that surfactant applied in electroless bath served to stabilize the suspension and improve the dispersion of TiO_2 . Areas of bright contrast found in this image may be associated to high atomic number (Z) elements, like Ti in TiO_2, whereas dark areas may relate to phosphorous-rich domains of the Ni-P matrix (Zarebidaki and Allahkaram, 2011).

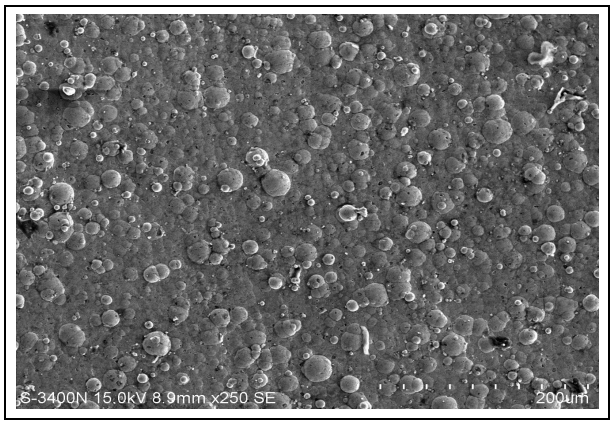

Fig. 7: Surface morphology of coated substrate

The elemental composition of the Ni-P-TiO_2 electroless composite coating was further confirmed by the EDS analysis. Having a high Ni content led to a more reliable metallic matrix with improved corrosion and mechanical properties in the presence of phosphorus. The presence of titanium and oxygen confirms the co-deposition of TiO_2 particles inserted homogeneously under SEM observation. The quantitative EDS analysis confirms that Ni is the major component (in weight % 90.21%), suggesting a heavily loaded Ni-matrix that can be expected for electroless Ni-P coatings. Phosphorus

content of this Ni-P is 6.83%, which belongs to medium or high phosphorus Ni-P coatings. This phosphorus level can be related to more amorphous or semi-amorphous microstructure for improved corrosion resistance and hardness. Titanium is detected at 0.98% confirming the presence of TiO_2 particles into the coating. Although these amounts are small, they are still enough to make a large contribution to wear resistance, hardness, and photocatalytic activity in the indicated field. According to the inset in Fig. 8, O (1.98%) can more support TiO_2 (Ti (oxides) since the ideal atomic ratio of Ti to O is 1:2.

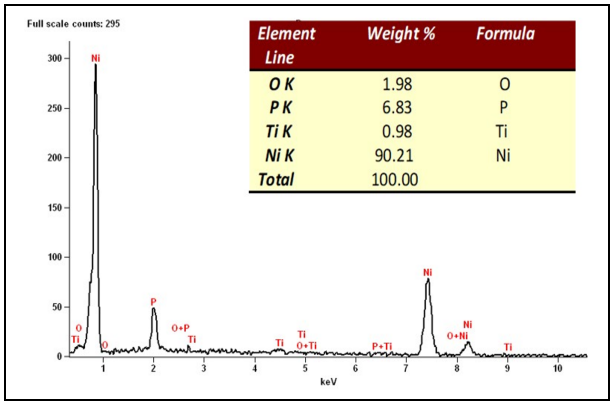

Fig. 8: Elements identified using EDAX on the deposits

Fig. 8 shows the EDS mapping of the Ni-P-TiO_2 electroless coating, representing the distribution of four main elements, Nickel (Ni), Phosphorous (P), Oxygen (O), and Titanium (Ti). Mapping of elements is shown in Fig. 9. Each map is for the Kα X-ray emission of the element, collected over an area indicated by the 10 µm scale bar. The Ni map (Ni) (Fig. 9a) is uniform and dense in the full field, which suggests contiguous and homogeneous Ni matrix in the coating. This indicates that the deposition of metallic layer is formed with only a small number of gaps or phase separation by the electroless deposition. The P map (Fig. 9b) also exhibits homogenous but slightly coarse distribution, which can be attributed to the conventional Ni-P alloy, when the phosphorus is co-deposited by chemical reduction method with the nickel. Map linked with O has more dispersed patterns with lower intensity and occurrence frequency of signals compared to the CH_4 map (Fig. 9c). This is indicative of oxygen being located at specific sites, which are likely to be the TiO_2 particles within the coating, or oxide-rich grain boundaries. The Ti map also displays a scattered distribution with intermediate levels of regularity, indicating the even dispersion of TiO_2 particles in the Ni-P matrix (Fig. 9d). The fact that Ti and O sites strongly overlap in space is clear evidence of the presence of TiO_2 rather than metallic Ti. Thus, these maps demonstrate the existence and co-localization of all the main components in the Ni-P-TiO_2 coating. Generally, there is a uniform distribution of Ti and O; if it happens at low amounts, then it suggests stable suspension of particles and efficient deposition, which is possibly also favored by the use of a surfactant during the process. This lack of heterogeneity is important in terms of having homogeneous mechanical and corrosion resistance properties of the coating (Chen *et al.* 2016).

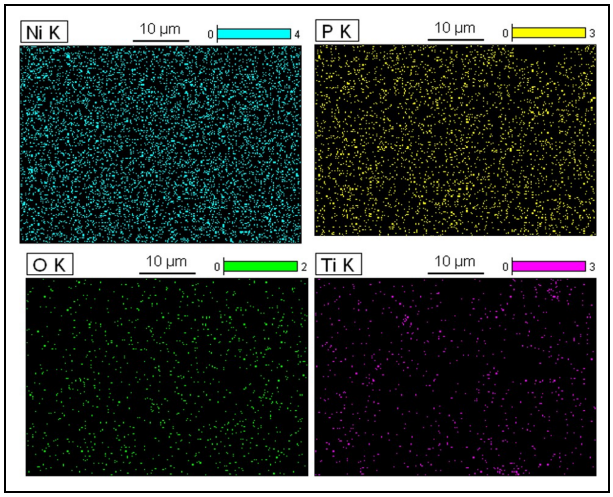

Fig. 9: Mapping of elements identified after eliminating the minor elements

The Rockwell C indentation test remains a well-accepted qualitative method for the evaluation of the adhesion strength of hard coatings according to the German standard DIN EN ISO 26443 (previous DIN 58196) and VDI 3198. Such patterns are compared with standard reference images (categorized HF1 to HF6) according to the VDI 3198 classification, with HF1 representing perfect adhesion (no cracks or delamination) and HF6 poor adhesion with heavy delamination and cracking. The current image shows several radial cracks and some of delamination, but the damage appears limited, as the coating still covers most of the indentation (Fig. 10). According to VDI 3198, this failure mode is closest to an HF3 class, which means adhesion was acceptable. Nevertheless, heat treatment can improve the interfacial bonding by retarding the crack propagation under stress (Shozib *et al.* 2021).

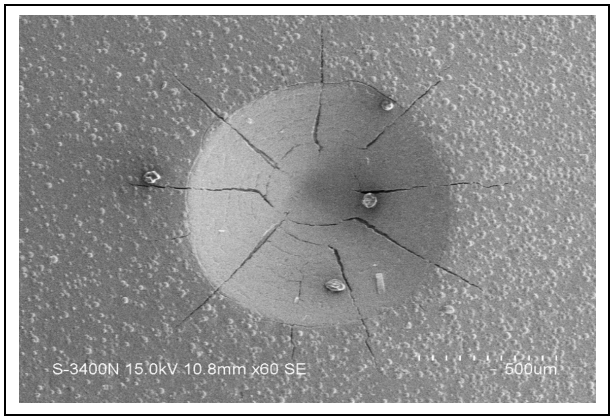

Fig. 10: Indentation on the deposit to study the quality of the coating

The phase and crystalline structure of the Ni-P-TiO_2 electroless coated is shown in the X-ray diffraction (XRD) pattern (Fig 11). Diffractogram shows set of peaks related to the major ingredients of the composite coating. The strongest peak can be observed at about $2\theta \approx 44.5°$, which is assigned to the Ni (111) plane, suggesting Ni as the major phase, and has a face-centred cubic crystal structure. The sharp intensity of this peak indicates a well-defined crystal state for capped Ni matrix. In addition, the peaks at $2\theta \approx 38.5°$ and $2\theta \approx 56.0°$ are indexed to TiO_2 (112) and Ni_3P (112), respectively. The peak corresponding to TiO_2 shows the existence of titanium dioxide particles in the coating, which can possibly enhance the mechanical and wear properties due to high hardness and stability of TiO_2 (Shozib *et al.* 2021). In a similar pattern, the $Ni_{12}P_5$ (204) reflection appears at $\sim 2\theta \approx 78.5°$ which indeed confirms that the nickel phosphide phases form within the structure, suggesting that phosphorus is not limited to solid solution and also reacts to form the intermetallic compounds. Such nickel phosphides are utilized to improve hardness and the corrosion resistance of the coating.

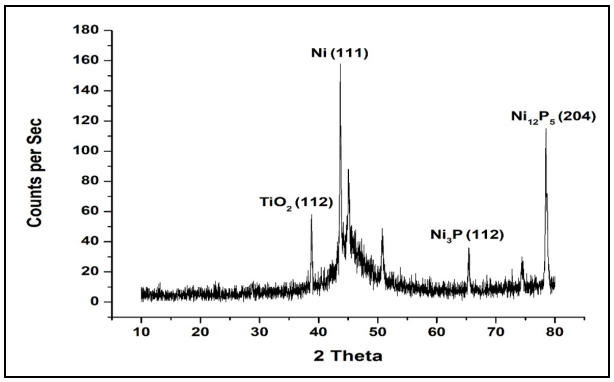

Fig. 11. Diffractogram of the deposit developed for optimized condition

5. CONCLUSION

This study established a predictive optimization framework for electroless Ni–P coatings on AH36 steel. Nanoparticle concentration was identified as the most influential factor on coating thickness, with 1.5 g providing the highest deposition due to improved TiO_2 support and dispersion. Surface roughness was primarily controlled by the reducing agent, with 30–35 g/L producing the smoothest surfaces. The surfactant not only enhanced nanoparticle dispersion but also contributed to surface planarization, with 1.2 g yielding the best results without destabilizing the bath. Interaction and 3D contour analyses confirmed strong non-linear and interdependent effects among the parameters, highlighting the need for multivariable optimization. The optimal combination (1.5 g nanoparticles, 1.2 g surfactant, and 40 g/L reducing agent) produced the highest Grey relational grade (0.76), representing the best balance between increased coating thickness and reduced roughness. Although the regression models did not achieve full statistical significance, they remain useful for directional prediction of coating performance. Validation experiments confirmed improved coating quality and homogeneous nanoparticle distribution, supporting the model's reliability. These results, not previously reported for AH36 steel, provide practical predictive tools for designing coating conditions and advancing surface engineering strategies in marine defence applications.

FUNDING

This research received no specific grant from any funding agency in the public, commercial, or not-for-profit sectors.

CONFLICTS OF INTEREST

The authors declare that there is no conflict of interest.

COPYRIGHT

REFERENCES

Alam, N. S. and Singh, H., Development of copper-based metal matrix composites: An analysis by SEM, EDS and XRD, *Microsc. Anal*., 28(4), 8–13 (2014).

Chen, D., Zhang, Y., Bessho, T., Sang, J., Hirahara, H., Mori, K. and Kang, Z., Layer by layer electroless deposition: An efficient route for preparing adhesion-enhanced metallic coatings on plastic surfaces, *Chem. Eng. J.,* 303, 100–108 (2016). https://doi.org/10.1016/j.cej.2016.05.114

Hadipour, A., Monirvaghefi, S. M. and Bahrololoom, M. E., Electroless deposition of graded Ni – P coatings, *Surf. Eng.,* 31(6), 399–405 (2015). https://doi.org/10.1179/1743294414Y.0000000430

Hao, Z., Zhang, Z., Zhou, W., Zhang, S., Ma, T., Wei, H., Wang, G., Wang, Q., Wang, L. and Li, R., Progress of material degradation: metals and polymers in deep-sea environments, *Corros. Rev*., 43(3), 315–334 (2024). https://doi.org/10.1515/corrrev-2024-0009

Jeyaganesh, D., Ziout, A., Qudeiri, J. A., Optimization of P-GMAW parameters using Grey relational analysis and Taguchi method, *Proc. 2021 IEEE 12th Int. Conf. Mech. Intell. Manuf. Technol*., 191–196 (2021). https://doi.org/10.1109/ICMIMT52186.2021.9476176

Krishnakumar, V. and Elansezhian, R., Wear and corrosion behavior of electroless Ni-P- TiO_2- Al_2O_3 nanocomposite coatings on magnesium AZ91D alloy, *Iop Conf. Ser., Mater. Sci. Eng*., 912, 052020 (2020). https://doi.org/10.1088/1757-899X/912/5/052020

Kuo, Y., Yang, T. and Huang, G. W., The use of a grey-based Taguchi method for optimizing multi-response simulation problems, *Eng. Optim*., 40(6), 517–528 (2008). https://doi.org/10.1080/03052150701857645

Rosas-Laverde, M. N., Pruna, A., Cembrero, J., Pascual, M. and Orozco-Messana, J., Optimizing Electroless Plating of Ni–Mo–P Coatings Toward Functional Ceramics, *Acta Metall. Sin*., 33, 437–445 (2020). https://doi.org/10.1007/s40195-019-00989-x

Salicio-Paz, A., Ugarte, I., Sort, J., Pellicer, E. and García-Lecina, E., Full Optimization of an Electroless Nickel Solution: Boosting the Performance of Low-Phosphorous Coatings, *Mater.,* 14(6), 1501 (2021). https://doi.org/10.3390/MA14061501

Sarkar, S., Baranwal, R. K., Nandi, R., Dastidar, M. G., De, J. and Majumdar, G., Parametric Optimization of Surface Roughness of Electroless Ni-P Coating, *Optimiz. Methods Eng.*, 197–207 (2020). https://doi.org/10.1007/978-981-15-4550-4_12

Selvan, R. A. S., Thakur, D. G., Seeman, M. and Naik, M., Surface Modification of AH36 Steel Using ENi-P-nano TiO_2 Composite Coatings Through ANN-Based Modelling and Prediction, *J. Mar. Sci. Appl.,* 21, 193–203 (2022). https://doi.org/10.1007/s11804-022-00288-5

Selvan, R. A. S., Thakur, D. G., Seeman, M., Balasubramanian, V. and Muraliraja, R., Optimisation and analysis of jet impingement erosion behaviour of composite titanium based electroless nickel ENi-P coated naval steel (AH36), *Trans. Inst. Met. Finish.,* 101(3), 140–149 (2023). https://doi.org/10.1080/00202967.2023.2185972

Senthilkumar, S., Karthick, A., Madavan, R., Moshi, A. M., Bharathi, S. R. S., Saroja, S. and Dhanalakshmi, C. S., Optimization of transformer oil blended with natural ester oils using Taguchi-based grey relational analysis, *Fuel,* 288, 119629 (2021). https://doi.org/10.1016/j.fuel.2020.119629

Shahzad, K., Fayyad, E. M., Nawaz, M., Fayyaz, O., Shakoor, R. A., Hassan, M. K., Umer, M. A., Baig, M. N., Raza, A. and Abdullah, A. M., Corrosion and Heat Treatment Study of Electroless NiP-Ti Nanocomposite Coatings Deposited on HSLA Steel, *Nanomater.,* 10(10), 1932 (2020). https://doi.org/10.3390/NANO10101932

Shozib, I. A., Ahmad, A., Rahaman, S. A. M., Abdul-Rani, M. A., Alam, A. M., Beheshti, M. and Taufiqurrahman, I., Modelling and optimization of microhardness of electroless Ni–P–TiO_2 composite coating based on machine learning approaches and RSM, *J. Mater. Res. Technol.,* 12, 1010–1025 (2021). https://doi.org/10.1016/J.JMRT.2021.03.063

Srivastwa, A. K., Sarkar, S., De, J. and Majumdar, G., Parametric optimization of electroless Ni-P-CNT coating using genetic algorithm to maximize the rate of deposition, *Mater. Today Proc.,* 66, 3769–3774 (2022). https://doi.org/10.1016/J.MATPR.2022.06.106

Thiemig, D. and Bund, A., Characterization of electrodeposited Ni-TiO_2 nanocomposite coatings, *Surf. Coat. Technol.,* 202(13), 2976–2984 (2008). https://doi.org/10.1016/j.surfcoat.2007.10.035

Venkatesh, C. and Venkatesan, R., Optimization of process parameters of hot extrusion of SiC/Al 6061 composite using Taguchi's technique and upper bound technique, *Mater. Manuf. Proc.,* 30(1), 85–92 (2015). https://doi.org/10.1080/10426914.2014.962658

Vijayanand, M., Varahamoorthi, R., Kumaradhas, P., Sivamani, S. and Kulkarni, M. V., Regression-BPNN modelling of surfactant concentration effects in electroless NiB coating and optimization using genetic algorithm, *Surf. Coat. Technol.,* 409, 126878 (2021). https://doi.org/10.1016/J.SURFCOAT.2021.126878

Zarebidaki, A. and Allahkaram, S. R., Effect of surfactant on the fabrication and characterization of Ni-P-CNT composite coatings, *J. Alloys Compd.,* 509(5), 1836–1840 (2011). https://doi.org/10.1016/j.jallcom.2010.10.057

Zhang, W., Cao, D., Qiao, Y., He, Z., Wang, Y., Li, X. and Gao, W., Microstructure and properties of duplex Ni-P-TiO2/Ni-P nanocomposite coatings, *Mater. Res*., 22(2), e20180748 (2019). https://doi.org/10.1590/1980-5373-MR-2018-0748

Zhu, M., Chen, Y., Chen, Y. and Hu, K., Application of Taguchi-grey relational analysis for optimizing process parameters of laser cladding for 316L stainless steel, *Int. J. Interact. Des. Manuf.,* 19, 6417–6428 (2025). https://doi.org/10.1007/s12008-024-02218-x